Harmonic Langmuir waves. III. Vlasov simulation

AUTHOR(S):

Umeda, T; Omura, Y; Yoon, PH; Gaelzer, R; Matsumoto, H

CITATION:

Umeda, T ...[et al]. Harmonic Langmuir waves. III. Vlasov simulation. PHYSICS OF PLASMAS 2003, 10(2): 382-391

ISSUE DATE:

2003-02

URL:

http://hdl.handle.net/2433/39792

PHYSICS OF PLASMAS VOLUME 10, NUMBER 2 FEBRUARY 2003

Harmonic Langmuir waves. III. Vlasov simulation

T. Umeda and Y. Omura
Radio Atmospheric Science Center, Kyoto University, Kyoto, Japan

P. H. Yoon
Radio Atmospheric Science Center, Kyoto University, Kyoto, Japan
and Institute for Physical Science and Technology, University of Maryland, College Park, Maryland 20742-2431

R. Gaelzer[a)]
Institute for Physical Science and Technology, University of Maryland, College Park, Maryland 20742-2431

H. Matsumoto
Radio Atmospheric Science Center, Kyoto University, Kyoto, Japan

(Received 29 August 2002; accepted 19 November 2002)

Generation of harmonic Langmuir modes during beam–plasma interaction is studied by means of nonlinear theoretical calculations and computer simulations. The present Vlasov simulation of multiple harmonic Langmuir modes (up to 12th harmonics), generalizes the previously available simulations which were restricted to the second harmonic only. The frequency-wave-number spectrum obtained by taking the Fourier transformation of simulated electric field both in time and space shows an excellent agreement with the theoretical nonlinear dispersion relations for harmonic Langmuir waves. The saturated wave amplitude features a quasi-power-law spectrum which reveals that the harmonic generation process may be an integral part of the Langmuir turbulence. © *2003 American Institute of Physics.* [DOI: 10.1063/1.1537240]

I. INTRODUCTION

Since the early days of computer simulations of plasma processes, the beam–plasma interaction has attracted a great deal of interest, since it is one of the simplest plasma instabilities. By the same token, the beam–plasma instability has also played a key role in the development of nonlinear plasma theories.

One of the earliest and simplest self-consistent theories developed for the beam–plasma interaction is the quasilinear theory,[1–3] followed by a more sophisticated version known as the weak turbulence theory.[4–10] The underlying assumption in these theories is the random-phased, incoherent nature of the fluctuations.

Meanwhile, early computer simulations of the beam–plasma instability[11–14] demonstrated that the dominant stabilization mechanism appeared to be the particle trapping in coherent nonlinear phase–space vortex. This led to attempts toward coherent nonlinear theories for the beam–plasma instability[15–21] on the one hand, and efforts to incorporate the coherent nonlinear physics into the kinetic theory, on the other. The various attempts to improve upon the renormalized kinetic theories, best exemplify the latter effort.[22–28]

We now know, thanks to more recent improved simulations,[29–31] that both the incoherent and coherent processes have roles to play in actual situations. By and large, if the beam density is sufficiently low and the initial velocity spread associated with the beam is sufficiently large, then quasilinear/weak turbulence theory is a valid first-order approach. For instance, in a recent article, Omura *et al.*[31] discuss the various situations regarding the preponderance of coherent versus incoherent nonlinear physics in regards to the beam–plasma interactions.

Given such a long history, one would think that the beam–plasma interaction is one of the most well-understood problems. However, there are still some outstanding issues, a prominent example being the generation of harmonics of plasma frequency.[13,17,18,32–53] The historical backdrop of this problem was briefly reviewed in the Introduction of paper I of this series [P. H. Yoon *et al.*, Phys. Plasmas **10**, 364 (2003)] and the physical significance of investigating such a problem was discussed in paper II [R. Gaelzer *et al.*, Phys. Plasmas **10**, 373 (2003)]. Therefore, these will not be repeated here.

In paper I of the present series, the nonlinear dispersion relations for the harmonic Langmuir waves were derived and, one of the results from the present paper, which comprises paper III, was previewed in order to make a concrete comparison with the theoretical dispersion curves. Then, in paper II, we formulated and numerically solved the theoretical wave and particle kinetic equations, with the aim of obtaining the saturated wave spectrum with a quasi-power-law-type feature. It was found that under a plausible initial condition, one of the solutions represented a power-law-type spectrum for the wave intensity. The purpose of the present paper is to discuss, in a comprehensive manner, the full details of the Vlasov simulation results.

II. VLASOV SIMULATION

We developed a Vlasov simulation code, which solves a one-dimensional Vlasov equation without the magnetic field,

[a)]CNPq fellow. Permanent address: Instituto de Física e Matemática, Universidade Federal de Pelotas (UFPel), Caixa Postal 354, 96010-900 Pelotas, RS, Brazil.

$$\frac{\partial f_s}{\partial t}+v_x\frac{\partial f_s}{\partial x}+\frac{q_s}{m_s}E_x\frac{\partial f_s}{\partial v_x}=0, \tag{1}$$

where the subscript s represents particle species (e.g., $s=e$ for the background electrons, $s=b$ for the beam electrons, and $s=i$ for the ions). The time-advancement numerical algorithm called "the splitting method" proposed by Cheng and Knorr[54,55] was adopted in our numerical scheme, and the Vlasov equation (1) is solved in fractional time steps by shifting the distribution function in the following manner:

$$\begin{aligned} f_s^{t_1}(x,v_x)&=f_s^{t}(x-v_x\Delta t/2,v_x),\\ f_s^{t_2}(x,v_x)&=f_s^{t_1}\left[x,v_x-\frac{e_s}{m_s}E_x^{t_1}(x)\Delta t\right],\\ f_s^{t+\Delta t}(x,v_x)&=f_s^{t_2}(x-v_x\Delta t/2,v_x). \end{aligned} \tag{2}$$

That is, we first advance the system in x direction over a half-time step, $t_1-t\equiv\Delta t/2$, compute the electric field from Poisson's equation,

$$\frac{\partial E_x^{t_1}(x)}{\partial x}=4\pi\rho^{t_1}(x)=4\pi\sum_s q_s\int_{-\infty}^{\infty}dv_x f_s^{t_1}(x,v_x), \tag{3}$$

make use of the updated electric field, E^{t_1}, to advance the system in v_x direction over a full time step, $t_2-t_1\equiv\Delta t$, and finally complete the time-stepping procedure by advancing the system along x direction for another half-time step, $\Delta t/2$. In order to solve Eq. (2) with high accuracy, we employed the cubic interpolated propagation (CIP) scheme.[56,57]

The velocity distribution function is discretized over the $x-v_x$ phase space with $N_x\times N_{v_x}=1024\times512$ cells. Periodic boundary conditions are imposed at both ends of the simulation box. The system length is $L_x=256\lambda_e$, where $\lambda_e=V_{te}/(\sqrt{2}\omega_{pe})$ is the initial Debye length. Here $V_{te}=\sqrt{2k_BT_e/m_e}$ is the thermal speed associated with the thermal background electrons, k_B, T_e, and m_e being the Boltzmann constant, electron temperature and mass, respectively. The plasma frequency, ω_{pe} is defined by $\omega_{pe}^2=4\pi n_e q_e^2/m_e$, where n_e and q_e represent the density and unit charge of the species $s=e$, i.e., the thermal electrons. The maximum and minimum velocities considered in the simulation are given, respectively, by $v_{\max}=7V_{te}$ and $v_{\min}=-7V_{te}$. Thus the grid spacing in the x and v_x directions are given, respectively, by $\Delta x=0.25\lambda_e$ and $\Delta v_x=0.0277V_{te}$. The time step is $\Delta t=0.01/\omega_{pe}$.

The initial configuration in the present study comprises of a weak electron beam drifting against the background thermal electrons. The density ratio of the beam electrons to the background electrons is given by $n_b/n_e=\omega_{pb}^2/\omega_{pe}^2=0.001$, where ω_{pb} is the plasma frequency associated with the beam component, defined by $\omega_{pb}^2=4\pi n_b q_b^2/m_b$. Here, of course, $q_b=q_e=-e$ and $m_b=m_e$. The initial thermal and drift velocities associated with the beam electrons are given, respectively, by $V_{tb}=0.5V_{te}$ and $V_d=3.5V_{te}$. The ion dynamics are not considered in the present simulation. They are assumed to form an immobile positively charged background.

In order to initiate the electron beam–plasma instability process, the seed perturbation must be imposed at the outset. This is accomplished in our simulation by the initial charge density (i.e., electron density) perturbation, which is modulated with a charge-neutral function,

$$n_1(x)/n_0=\sum_{i=1}^{N_x/2}A(k_i)\cos(k_ix+\psi_i), \tag{4}$$

where $\psi_i=2\pi R_i$ with R_i being a uniformly distributed random number, $0\leqslant R_i<1$. The difference equation of Eq. (3) is given by

$$\frac{E_x(i)-E_x(i-1)}{\Delta x}=2\pi[\rho(i)+\rho(i-1)]. \tag{5}$$

By taking the Fourier transformation of the above difference equation, we obtain that the amplitude of each wave mode $A(k_i)$ takes the following form:

$$\begin{aligned} A(k_i)&=\frac{K_i|E_x(k_i)|}{\cos[k_i(\Delta x/2)]},\\ K_i&=\frac{\sin[k_i(\Delta x/2)]}{k_i(\Delta x/2)}. \end{aligned} \tag{6}$$

In the present simulation the spectral shape of the initial noise is chosen to be in a power-law form, although other choices can also be made,

$$\log_{10}|E_x(k_i)|=-\alpha-\beta\log_{10}k_i \tag{7}$$

for

$$i=1\sim N_x/2.$$

Finally, we note that the discretized wave number, k_i, is related to the unit wave number increment, Δk, by $k_i=i\Delta k$ where $\Delta k=k_1=2\pi/L_x$. Specifically, the parameters of the power-law spectrum presented in this paper are $\alpha=4.0$, $\beta=2.5$.

III. BRIEF OVERVIEW OF HARMONIC LANGMUIR WAVE THEORY

In paper I, we derived the nonlinear dispersion relation for the harmonic Langmuir waves on the basis of theoretical analysis of nonlinear plasma spectral balance equation. For a one-dimensional beam–plasma system where the Langmuir waves are excited by an interaction of a background plasma of temperature T_e, and a tenuous electron beam with average drift speed V_d and beam temperature T_b, the desired dispersion relation for the harmonic Langmuir waves is given by

$$\begin{aligned} \frac{\omega_{k_x}^{Ln}}{\omega_{pe}}&=n+\frac{3k_x^2V_{te}^2}{2\omega_{pe}^2}-\frac{3(n-1)\,k_{L1}^2V_{te}^2}{\omega_{pe}^2}\left(\frac{k_x}{k_{L1}}-\frac{n}{2}\right),\\ k_{L1}&=\omega_{pe}/(V_d-V_{tb}). \end{aligned} \tag{8}$$

We also obtained an analytical expression for the instantaneous growth rate of the harmonic Langmuir waves, given by

$$\frac{\gamma_{k_x}^{Ln}}{\omega_{pe}} = -\frac{\sqrt{\pi}}{2^{3/2}}\left(\frac{\omega_{k_x}^{Ln}}{kV_{te}}\right)^3\left[\frac{\omega_{k_x}^{Ln}}{\omega_{pe}}\exp\left(-\frac{(\omega_{k_x}^{Ln})^2}{2k_x^2V_{te}^2}\right)\right.$$
$$\left. + \frac{n_b}{n_e}\left(\frac{V_{te}}{V_{tb}}\right)^3\frac{\omega_{k_x}^{Ln}-k_xV_d}{\omega_{pe}}\exp\left(-\frac{(\omega_{k_x}^{Ln}-k_xV_d)^2}{2k_x^2V_{tb}^2}\right)\right]. \tag{9}$$

However, for the fundamental Langmuir mode, $L1$, a more accurate linear growth rate can be obtained directly from the full transcendental dispersion equation,

$$0 = 1 - \frac{\omega_{pe}^2}{k_x^2V_{te}^2}Z'(\zeta_e) - \frac{\omega_{pb}^2}{k_x^2V_{tb}^2}Z'(\zeta_b),$$
$$\zeta_e = \frac{\omega}{k_xV_{te}}, \quad \zeta_b = \frac{\omega - k_xV_d}{k_xV_{tb}}. \tag{10}$$

In the above, $Z(z)$ is the Fried–Conte plasma dispersion function, the prime indicating the derivative with respect to the argument. The complex root of the above equation, $\omega = \mathrm{Re}\,\omega + i\,\mathrm{Im}\,\omega$, can be used to replace the analytical expressions for the $L1$ mode dispersion relation and the growth rate, $\mathrm{Re}\,\omega = \omega_{k_x}^{L1}$ and $\mathrm{Im}\,\omega = \gamma_{k_x}^{L1}$, respectively.

In addition to the dispersion relations and instantaneous growth rates, we also derived and numerically solved the self-consistent particle and wave kinetic equations. The wave kinetic equation adopted in the theoretical computation included full nonlinear wave coupling terms, but for the time period of interest to us, the dynamics of the system is practically governed by the quasilinear theory. The electron quasilinear kinetic equation is the well-known diffusion equation, while the quasilinear wave kinetic equations for the harmonic Langmuir waves, including the fundamental, are essentially governed by the induced emission/absorption process. The self-consistent dynamic equations in one-dimensional situation is thus, given by

$$\frac{\partial f_e}{\partial t} = \frac{\pi^2e^2}{m_e^2}\frac{\partial}{\partial v_x}\sum_{\sigma=\pm1}\sum_{n=1,2,\ldots}\int dk_x\, I_{Ln}^{\sigma}(k_x)$$
$$\times\delta(\sigma\omega_{k_x}^{Ln} - k_xv_x)\frac{\partial f_e}{\partial v_x},$$
$$\frac{\partial I_{Ln}^{\sigma}(k_x)}{\partial t} = n^2\pi(\sigma\omega_{k_x}^{Ln})\frac{\omega_{pe}^2}{k_x}\int dv_x$$
$$\times\delta(\sigma\omega_{k_x}^{Ln} - k_xv_x)\frac{\partial f_e}{\partial v_x}I_{Ln}^{\sigma}(k_x) \quad (n=1,2,3,\ldots). \tag{11}$$

In the above, $I_{Ln}^{\sigma}(k_x)$ stands for the square of the wave electric field for the nth harmonic Langmuir mode, $I_{Ln}^{\sigma}(k_x) = |E_x^n(k_x)|^2$, and the sign of σ signifies the direction of the wave phase speed. The numerical solutions of theoretical equations were already presented in papers I and II, and thus shall not be repeated here. However, as appropriate, we will refer to the theoretical results and make comparisons with the simulation results.

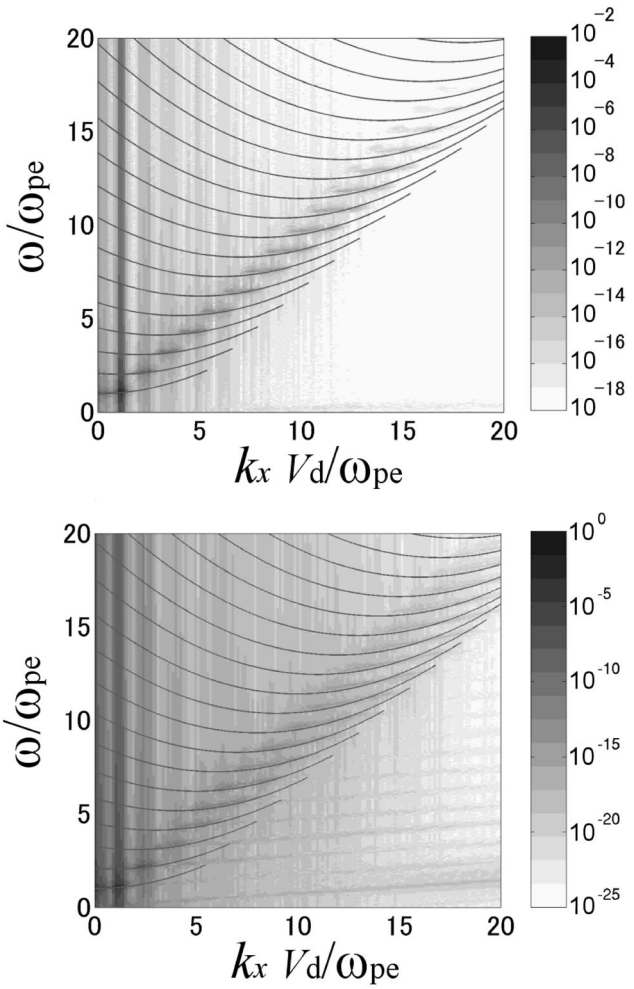

FIG. 1. Numerically simulated $\omega - k_x$ diagram, which is generated by plotting the wave intensity, $|E_x(\omega,k_x)|^2$, in grayscale versus ω and k_x. In the first case, the data were collected over a time period ranging from $\omega_{pe}t = 409.6$ to $\omega_{pe}t = 512.0$. The second case corresponds to $819.2 < \omega_{pe}t < 921.6$. The instensity is normalized by the thermal energy of the background electrons $n_em_eV_{te}^2/2$. The solid lines show the linear and nonlinear dispersion curves obtained from Eq. (8).

IV. SIMULATION RESULT

In Fig. 1 we plot an ω vs k_x diagram obtained by taking the Fourier transformation of electric field data in both space and time. This diagram shows $|E_x(\omega,k_x)|^2$ over an interval corresponding to two time periods, the first ranging from $\omega_{pe}t = 409.6$ to $\omega_{pe}t = 512.0$, and the second period ranging from $\omega_{pe}t = 819.2$ to 921.6. The intensity is normalized by the thermal energy density of the background electrons $n_em_eV_{te}^2/2 = (m_e\omega_{pe}V_{te})^2/(8\pi e^2)$.

To compare the present simulation result with the theory, we have superposed the theoretical dispersion curves, Eq. (8), on top of the simulated grayscale intensity plots in Fig. 1. In plotting this result, we have carefully estimated the actual thermal velocity of the background electrons, average drift velocity, and the thermal velocity of the beam electrons after the saturation of the instability ($\omega_{pe}t = 409.6$). This is because the theoretical dispersion relation (8) depends on the particle parameters, V_d, V_{te}, and V_{tb}. We could have simply used the initial values for these quantities, V_{te}

$=0.28V_d$, $V_{tb}=0.14V_d$, and still would have obtained a fairly reasonable agreement, but since both the background and beam electrons undergo slight heating, while the average beam speed decreases during the wave growth and saturation process, we have decided to improve upon the theoretical dispersion curve by computing the average values for these quantities during the time period of the simulation. We find that the numerically computed quantities correspond to $V'_{te}=0.28V_d$, $V'_{tb}=0.21V_d$, and $V'_d=0.96V_d$. This implies a decrease in average drift speed and a modest heating in the beam electrons. Making use of these refined electron speeds, we find an overall agreement between the nonlinear dispersion relation (8), and the Vlasov simulation result.

Graphical representation of the simulation results in ω vs k_x diagram format, as we do here, was not done in early simulations which reported Langmuir harmonic generation by beam–plasma instability.[45–51] The ω vs k_x plot is very informative, since without such a plot, one cannot fully characterize the true nature of the harmonic modes. In the absence of such an information, early interpretation of the harmonic generation tended to refer to these modes as a quasibeam mode, $\omega\approx k_xV_d$.

In recent works,[52,53] on the other hand, one can find similar representations of the simulation result such as our Fig. 1. However, Refs. 52 and 53 are limited to the first harmonic ($n=2$) only. In contrast, Fig. 1 shows not only the first harmonic but all higher harmonics up to $n=12$. Such a result has not been reported in the literature. A recent paper by Viñas *et al.*,[60] in which the authors simulated the response of an unmagnetized plasma as it is suddenly immersed to a field of high-amplitude ion-acoustic wave, on the other hand, it was shown that multiple harmonics of plasma oscillation frequency were excited. The resulting frequency-wave number dispersion diagram is qualitatively similar to our result, but the physical situation considered in Ref. 60 is obviously very different from the present discussion.

The $\omega-k_x$ diagram clearly shows that the harmonic Langmuir waves are not excited along the beam-mode line,

$$\omega=k_xV_d,$$

but are excited in $\omega-k_x$ space, dictated according to the nonlinear dispersion relation [see Eq. (8)],

$$\omega=\omega_{k_x}^{Ln}.$$

However, the actual amplification of nonlinear eigenmodes occurs only when the imaginary (which means that it is not an eigenmode, hence not supported by the plasma) quasibeam-mode line modified by thermal spread, $\omega=k_x(V_d\pm V_{tb})$, intersects with the eigenmode solutions, $\omega=\omega_{k_x}^{Ln}$.

Note that the intensity of higher harmonics decreases as the harmonic mode number increases such that beyond $n=12$, no discernable amplified intensity is apparent. We should note that the high harmonic modes possess very low intensity levels. As such, it would be very difficult to simulate these modes by means of the present-day particle-in-cell simulations owing to the high noise level intrinsic to the particle simulation. In this regard, the Vlasov simulation is an ideal tool to study the phenomenon of Langmuir turbulence involving the harmonic generation.

According to the simulated $\omega-k_x$ diagram in Fig. 1, the higher harmonics have incrementally broader ranges of wave numbers over which the modes are excited. This result is also in agreement with the theoretical growth rate property, Eq. (9), of the harmonic Langmuir modes (see Fig. 2 of paper I). However, we should also point out that the agreement between the theory and simulation in the case of the earlier time period, $409.6<\omega_{pe}t<512.0$, becomes better for the lower harmonics. As the harmonic mode number increases, on the other hand, the theoretical curves and simulated intensities begin to deviate somewhat, albeit only slightly. Specifically, the theoretical dispersion relations can be described as parabolas, whereas the simulated grayscale intensities can be characterized more or less as short straight lines. This is not too surprising since the theoretical curves are the result of an approximate analysis. We should note, however, that the sampling time domain of $\omega_{pe}t=409.6$ to $\omega_{pe}t=512.0$, still corresponds to relatively early time period during which the fluctuation is not completely random phased.

The second case, which corresponds to a later time, $819.2<\omega_{pe}t<921.6$, shows that the harmonic mode structure persists although the intensities of the modes have diminished somewhat. Note that the reasonable agreement between the theoretical dispersion curves, Eq. (8), and the simulation is not only maintained but is actually improved slightly, especially for the higher-harmonic modes. Again, this is not surprising, and can be easily explained, since the later time period corresponds to a more turbulent stage, in which the theoretical assumptions implicit in the derivation of Eq. (8) become increasingly more valid. In spite of this, however, we should also note that the agreement becomes increasingly poorer regardless of harmonic mode number, as one proceeds from lower k_x regime to higher and higher wave number domain. For high-k_x values, the simulated dispersion curves are no longer parabolas, but are more accurately described as straight lines.

Figure 2 shows the time evolution of the spectral wave energy density, $|E_x(t,k_x)|^2$ [normalized with respect to the same thermal energy density of the background electrons as before, namely, $n_em_eV_{te}^2/2=(m_e\omega_{pe}V_{te})^2/(8\pi e^2)$]. According to Fig. 2, appreciable enhancements of the electric field energy occur in the vicinities of wave numbers corresponding to $k_1V_d/\omega_{pe}=1.2$, $k_2V_d/\omega_{pe}=2.4$, $k_3V_d/\omega_{pe}=3.6$, $k_4V_d/\omega_{pe}=4.7$, $k_5V_d/\omega_{pe}=5.9$, $k_6V_d/\omega_{pe}=7.1$, and so on. When compared with Fig. 1, one may note that these values correspond to the central wave numbers for $L1$, $L2$, $L3$, ... modes. Consequently, k_1, k_2, k_3, ... correspond to the wave number at which the peak intensities of $L1$, $L2$, $L3$, ... modes take place.

It should be noted that, at first sight, the emergence of enhanced harmonic mode structure does not seem to take place until the system has evolved to $t\sim200\omega_{pe}^{-1}$, or so. However, this is only because the grayscale plot does not show very small intensities clearly. The subsequent figure will show that the harmonic modes do indeed emerge very

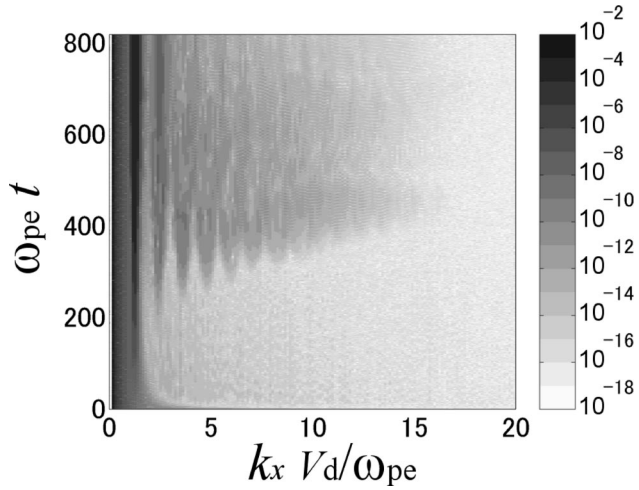

FIG. 2. Time evolution of the spectral wave energy density $|E_x(t,k_x)|^2$ normalized by the thermal energy of the background electrons $n_e m_e V_{te}^2/2$.

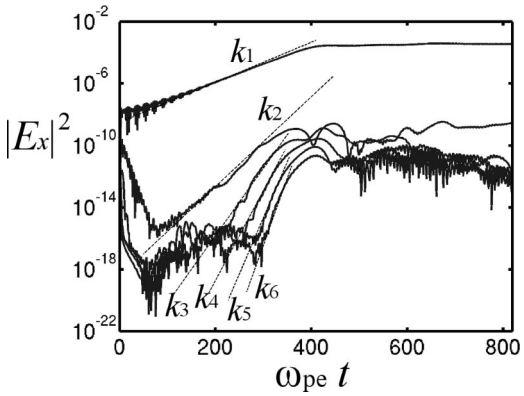

FIG. 3. Time history of electric field energy for the first six harmonic modes, $|E_x(k_n)|^2$ $(n=1,2,\ldots,6)$, where $k_1V_d/\omega_{pe}=1.2$, $k_2V_d/\omega_{pe}=2.4$, $k_3V_d/\omega_{pe}=3.6$, $k_4V_d/\omega_{pe}=4.7$, $k_5V_d/\omega_{pe}=5.9$ and $k_6V_d/\omega_{pe}=7.1$. The normalization is as before, i.e., with respect to the thermal energy of the background electrons, $n_e m_e V_{te}^2/2$. Straight lines represent the linear growth rate for each harmonic.

early on, in agreement with Refs. 47 and 49, where it is reported that the harmonics appear as early as a few plasma oscillation periods. In spite of the fact that physical parameters as well as the numerical algorithms adopted in our study are distinct from those of Refs. 47 and 49, it is remarkable that these works are in good overall agreement.

To understand the onset of the harmonics in more detail, we specifically chose the first six harmonic modes (with wave number corresponding to k_1, k_2, …, k_6) and plotted the time history of the wave energy density evolution for each mode. The result is displayed in Fig. 3. It can be seen that the fundamental Langmuir $(n=1)$ mode grows in an exponential fashion at the start of the simulation run. The linear theoretical prediction for $L1$ mode evolution is shown by the straight line. As one can see, the agreement is excellent. To improve upon the comparison between the theory and simulation, the theoretical growth rate was computed on the basis of the exact dispersion equation (10), rather than on the approximate analytical expression (9). We found that although the analytical formula does a good job of an overall description of the instability property, it nevertheless tends to overemphasize the actual growth rate. Therefore, we have decided to resort to the full solution of Eq. (10), which can be done for $L1$ mode. Thus, the maximum linear growth rate for $L1$ mode was determined by numerically solving Eq. (10). The subsequent growth rates for higher-harmonic modes were determined by simply multiplying the harmonic mode number to the $L1$ mode maximum growth rate. The result is a good overall agreement with the theory, although for harmonic modes corresponding to $n\geqslant 3$ the very early-time behavior of the modes is obscured by the sea of initial noise.

Note that for a brief period following the start of the simulation, the wave modes in k_n $(n\geqslant 2)$ initially decrease sharply. This occurs for a period of several tens of plasma oscillations, and is consistent with the similar behavior reported in Refs. 47 and 49. Since the wave energy at a given k_n is shared by the fundamental Langmuir mode as well as all the higher harmonics, the initial damping can be attributed to the Landau damping of $L1$ mode at those high k_n values. During the early time ($\omega_{pe}t$ less than 50 or so), the harmonic modes have not reached sufficiently high intensity to exhibit themselves above the $L1$ mode noise level.

At some later time, around $\omega_{pe}t\geqslant 50$ or so, the first harmonic mode $(n=2)$ begins to emerge from the background of initial noise. It is difficult to determine the precise initial level of $L2$ mode, since the mode emerges from the ambient background noise. However, once the mode exhibits itself above the noise, the subsequent amplification follows the theoretical prediction very well, as indicated by the straight line. Similar behavior can be discerned for higher harmonics, k_3, k_4, ..., etc.

To understand the physical origin of the early-time rapid damping of the initial noise, we have solved the theoretical equation (11) and plotted the result in Fig. 4, where the time history of electric field energy for the first four harmonic modes, $|E_x(k_n)|^2$ $(n=1,2,\ldots,4)$, similar to Fig. 3, is shown. The curves are computed on the basis of theoretical equation (11), and the solid lines represents the summation of all modes at each wave number, k_1, k_2, k_3, and k_4, which is equivalent to what is done with the simulation result. In contrast, the dotted line represents the true behavior of each harmonic. In the simulation, one cannot separate the contribution of one particular harmonic from all other harmonics, at a given wave number. Figure 1 of paper II is in the same format as the dotted lines of the present Fig. 3. As the solid curves demonstrate, the very early-time damping behavior of the cumulative mode intensities resemble the simulation result shown in Fig. 3 in a qualitative manner. From this, we believe that the comparison between the theory and simulation is rather good.

One might argue that, on the basis of Fig. 3 alone, it is difficult to ascertain whether the onset of harmonic modes takes place after some time has elapsed following the initial excitation of $L1$ mode, or whether they are all simultaneously "triggered" at the outset. However, on the basis of the excellent agreement between the theoretical quasilinear growth rate prediction (Fig. 4) and the dynamical behavior of

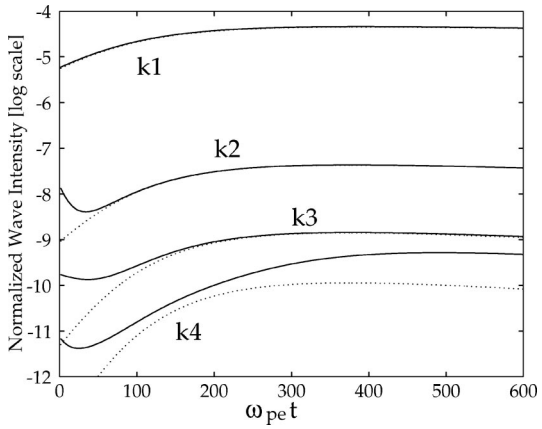

FIG. 4. Time history of electric field energy for the first four harmonic modes, $|E_x(k_n)|^2$ $(n=1,2,\ldots,4)$, similar to Fig. 3, but computed on the basis of theoretical equation (11). The solid line represents the summation of all modes at each wave number, k_1, k_2, k_3, and k_4, while the dotted line represents the true behavior of each harmonic. The very early-time behavior of the cumulative mode intensities resemble the simulation in a qualitative manner.

the harmonic modes as seen in the simulation (Fig. 3), it is reasonable to theorize that the harmonic modes were all present at time $t\approx 0$, but were hidden beneath the noise, and become apparent only after some time.

The generalized weak turbulence theory, as presented in paper II, assumes small but finite levels of harmonic modes at the outset. Although it is not possible to compute the initial noise level within the context of such a theory in a self-consistent manner, it is nevertheless plausible that the presence of $L1$ mode, however low its intensity may be, leads to the forced nonlinear perturbation which is rich in higher harmonic content. Such a concept was already quantitatively demonstrated in Refs. 17 and 18 in the context of coherent nonlinear theory. Thus, it is possible that a similar mechanism will provide the necessary seed perturbation level in the case of broadband turbulence theory, in close analogy with the coherent nonlinear theory,[17,18] although no such theory is available at the present time. In any case, it might be possible to explain the existence of the harmonic content at the outset naturally, by such a higher-order nonlinear theory.

We now show the time evolution of the distribution function in Figs. 5 and 6. The set of panels on the left show the average velocity distribution functions $N_x^{-1}\int dv_x\, f(x,v_x)$ at different times, while the panels on the right show the corresponding $x-v_x$ phase–space diagrams. At $\omega_{pe}t=204.8$, one may observe that the phase–space structure undulates with the characteristic wavelength corresponding to the dominant k_1 wave mode. However, subsequent evolution of the system exhibits the emergence of multiple striations associated with the phase–space structure. The fine structure, already evident at $\omega_{pe}t=307.2$, indicates the excitation of smaller-scale modes, i.e., the harmonics. At $\omega_{pe}t=409.6$, one can clearly see that nonlinear vortices undergo multiple folding upon itself. The largest-scale vortices are, of course, those corresponding to the dominant k_1 mode, but within the major vortices, one can discern the emergence of fine structure, which was already apparent at earlier times, but has now become obvious. Again, the existence of these fine structure is intimately related to the harmonic modes, as already noted.

In Fig. 6 we continue with the display of phase–space evolution for longer time periods. From the phase–space plots shown in Fig. 6, it can be said that the system has now entered a stage which can be characterized as genuinely turbulent. The time evolution of the averaged velocity space distribution is in agreement with the customary quasilinear plateau formation, as dictated by Eq. (11). According to Figs. 5 and 6, the full quasilinear saturation of the beam–plasma

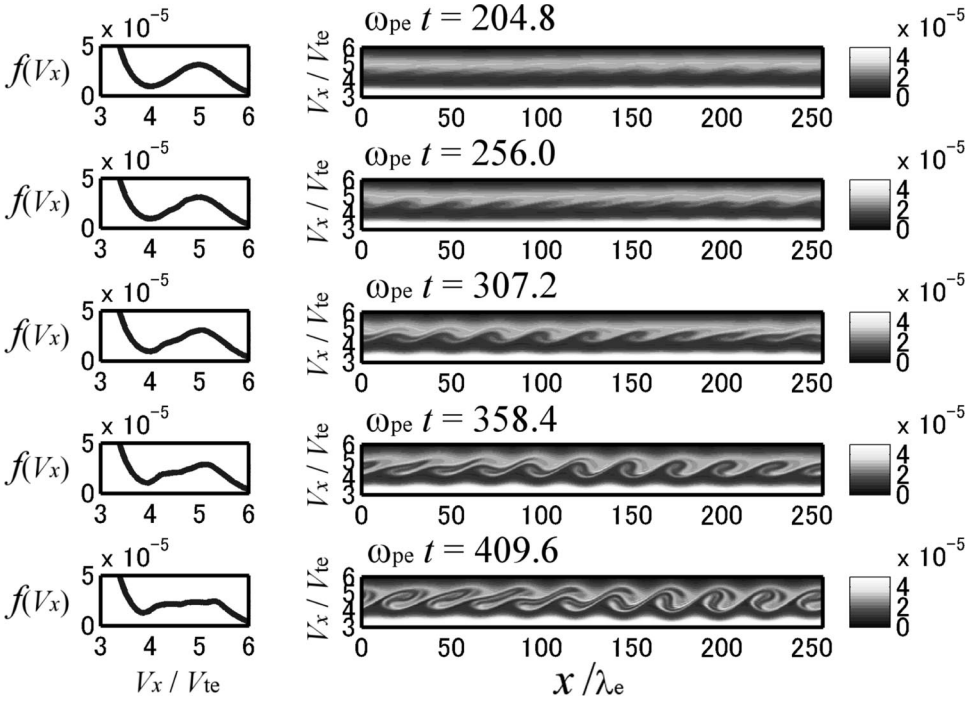

FIG. 5. The velocity space distrubution function, $N_x^{-1}\int dx\, f(x,v_x)$, at different times and the corresponding $x-v_x$ phase plots. Note that by the time the system has evolved to $\omega_{pe}t=409.6$, the phase–space plot shows that the perturbation is comprised of vortices with multiple folding pattern.

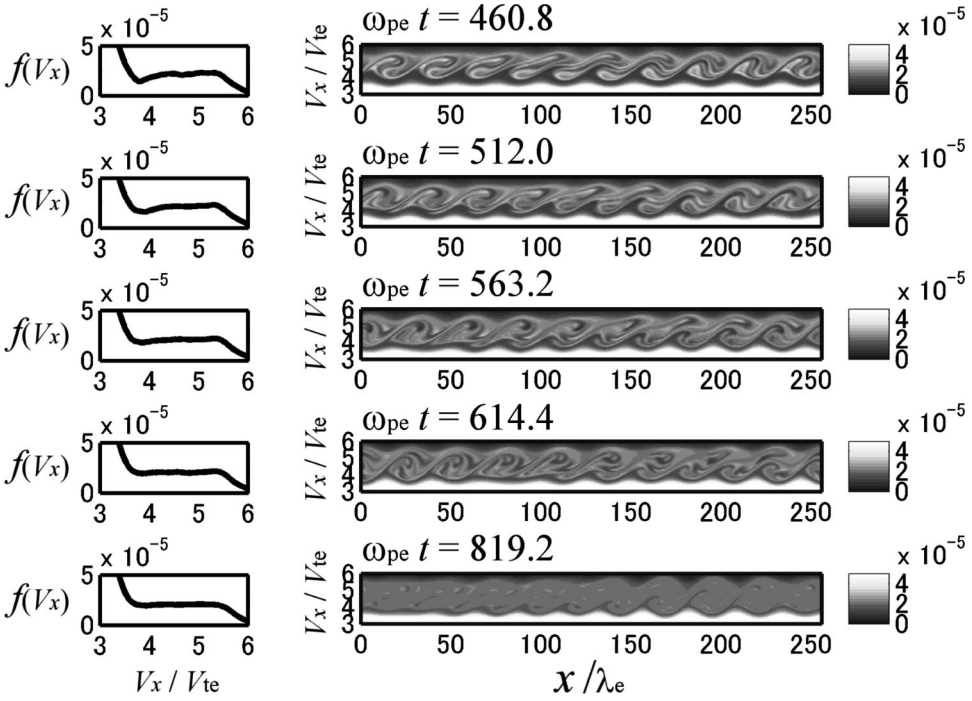

FIG. 6. Continuation of Fig. 5 for longer time periods. Note, on the basis of $x-v_x$ phase–space structure, that the entire time period, $460.8 \leqslant \omega_{pe}t \leqslant 819.2$ can be characterized as "turbulent."

instability is achieved near the end of the simulation run, namely, at $\omega_{pe}t=819.2$.

Studying the evolution of the beam–plasma system in phase–space, as shown in Figs. 5 and 6, can be very instructive in understanding the development of Langmuir turbulence. It demonstrates the transition from the laminar phase–space fluctuations at early time, say $\omega_{pe}t=204.8$, to a complicated vortex structure which contains smaller-scale structure within itself at later times. This is highly reminiscent of the development of turbulence in neutral fluids. As is well known, fluid turbulence involves the formation of eddies through shear-flow instability, e.g., the flow inside a pipe. The largest scale-size eddies are created as the shear in the fluid flow increases, followed by smaller-scale eddies, which are generated by the shear within the largest eddies themselves, thus giving rise to the Kolmogorov-type cascading process.

The Langmuir turbulence is different from fluid turbulence, of course, in that it involves microscopic wave-particle interaction (i.e., velocity space instability), and it involves no such thing as the configuration–space eddies. However, the $x-v_x$ phase–space vortex structure bears a morphological resemblance with the fluid turbulence in the sense that largest-scale structure (i.e., k_1 mode vortex) contains within itself, the fine structure. One should note, however, that the analogy with the fluid turbulence is only on a superficial level, since the Langmuir turbulence, as seen in Figs. 5 and 6, involves the excitation of harmonics, in which the process is essentially (quasi) linear in nature. In contrast, the fluid turbulence is a fully nonlinear process.

As we have already implied in the foregoing discussion, one of the important implications in the present study of harmonic Langmuir wave excitation is that one may understand the Langmuir turbulence through the light of harmonic generation, which is very different from the fluid turbulence. Authors of early papers on harmonic Langmuir wave generation[17,18,32,33] have already noted the potential significance of this process in understanding the turbulence in plasmas. As we will show below, the spectrum of harmonic Langmuir wave intensities form a quasi-power-law feature in the saturation stage. One of the ways to characterize a turbulence (in any medium) is to consider the quasistationary power-law spectrum. The reason why the power-law spectrum is of interest is that such a spectrum implies a quasi-scale-free structure associated with the turbulence. A good example of the scale-free structure is the well-known fractals. The power-law index characterizes the scaling property of the turbulence. For this reason, to obtain a scale-invariant Langmuir turbulence theory has been an ongoing effort (see the discussion in the Introduction of paper II). According to our theory and simulation, however, the power-law spectrum seems to be a natural byproduct of harmonic generation.

In Fig. 7 we plot the normalized wave electric field energy, $|E_x(k_x)|^2/n_e m_e V_{te}^2$, versus normalized wave number, $k_x V_d/\omega_{pe}$. The wave spectrum is plotted at intervals of $\omega_{pe}t=204.8$, 307.2, 409.6, and 819.2. The straight line indicates the power-law profile associated with initial wave intensity, which is given by a formula equivalent to Eq. (7). At $\omega_{pe}t=204.8$, the enhancement of k_1 mode is visible, while other wave modes are also seen to be emerging from the noise level. At $\omega_{pe}t=307.2$, the enhancements of the harmonic modes at k_2, k_3, etc., are more clearly visible, at least up to $n=5$. Note that the wave spectrum at this time can already be characterized by a power law. At $\omega_{pe}t=409.6$, the individual peaks are not so apparent because of the overlap of harmonic spectra. Moreover, the spectral shape deviates somewhat from the pure power law. However, this is only a transient behavior, and at the final time, $\omega_{pe}t=819.2$, it can be seen that the spectrum has settled down to a quasi-power-law with index ~ -5 to ~ -6.

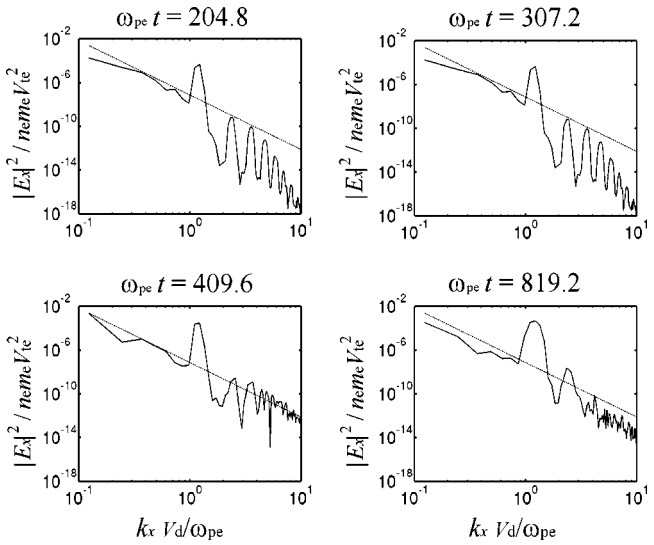

FIG. 7. Spectra of the normalized wave electric field energy, $2|E_x(k_x)|^2/n_e m_e V_{te}^2$, versus $k_x V_d/\omega_{pe}$, at $\omega_{pe}t=204.8$, 307.2, 409.6, and 819.2. The dashed line represents the initial profile of the wave intensity. Note that the final spectrum is roughly characterized by the initial power-law index of ~ -5.

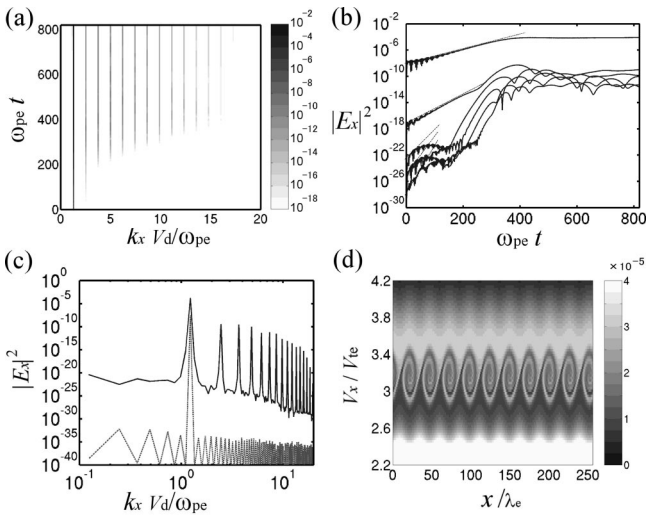

FIG. 8. This figure shows the case of coherent initial perturbation with a single wave mode at $k_x=k_1$. (a) Time evolution of spectral wave energy density, $|E_x(t,k_x)|^2$, versus time, $\omega_{pe}t$, in the same format as Fig. 2, (b) time history of the first six harmonic mode intensities in the same format as Fig. 3, (c) the evolution of wave spectrum, $|E_x(k_x)|^2$ versus k_x, at $\omega_{pe}t=0.0$ and 819.2, and (d) $x-v_x$ phase–space diagram at $\omega_{pe}t=409.6$.

It is interesting to compare the present finding to some earlier efforts, namely, those based upon the strong Langmuir turbulence theory. Ever since Zakharov proposed his theory which predicts $k^{-7/3}$ scaling associated with the collapsing Lagmuir caviton,[58] many have attempted to confirm such a scaling law. A good example is the work by Robinson and Newman.[59] However, the classical $-7/3$ power law is not found in their strong turbulence simulation, but instead, they find a scaling law close to k^{-4} or so. We caution the readers, however, that a direct comparison to our full Vlasov simulation is not very meaningful, since Zakharov equation is a simplified model equation.

A caveat in our interpretation of the final spectrum as a quasi-power-law is the following: As the reader may appreciate, the fundamental mode, $L1$, is characterized by a prominent peak which does not fall neatly along the simple power-law profile. We have thus excluded this $L1$-mode peak in the interpretation of the power-law distribution with an index equal to ~ -5 to ~ -6. We believe that the enhanced peak associated with the fundamental $L1$ mode is owing to the coherent particle trapping saturation mechanism, which tends to lead to higher saturation level than predicted by simple quasilinear theory.

In our simulations, we found that the high-end of the k_x spectrum, namely, those spectral ranges corresponding to $k_x V_d/\omega_{pe}>10$, or so, exhibits a slight steepening of the power-law distribution. This occured in all our simulation runs regardless of the initial conditions. Thus, we believe that it is owing to the grid-scale dissipation in the numerical scheme. This behavior is not shown in Fig. 7, since we restricted ourselves to the range, $10^{-1}<k_x V_d/\omega_{pe}<10$. However, in the next example, such a behavior will be clearly shown. In any case, it is interesting to note that such a feature is often present in many turbulent systems, such as in neutral fluid turbulence (strong turbulence simulation by Robinson and Newman[59] also shows this behavior), where it is known there as the dissipation range behavior. It is also interesting to note that in many real turbulent systems, the spectra often possess a prominant peak corresponding to low-frequency and large-scale coherent structure. Our simulated harmonic Langmuir wave spectrum possesses these features.

The overall power-law index of roughly ~ -5 to ~ -6 is also seen in the early beam–plasma experiment by Apel.[32,33] In the present simulation such a power-law index emerges quite naturally. One might note, however, that the initial wave spectrum which we implemented at the start is also of a power-law-type with the similar power-law index close to -5 or -6. Thus, one might naturally wonder whether the final result somehow reflects what was imposed at the outset. In order to see how robust the final outcome is, we have experimented with several different profiles associated with the initial noise, including different power-law indices (ranging from -1 to -6), white noise, and a monochromatic perturbation. The end result invariably seems to be a quasi-power-law with an approximate -5 to -6 index, although the detailed structure of the final spectrum (at $\omega_{pe}t=819.2$) is different from run to run.

As a concrete demonstration of this finding, we show in Fig. 8, the case of a monochromatic perturbation. In this run, we initiated the instability by imposing a sinusoidal perturbation with a single wave mode with $k_x=k_1$. Panel (a) shows the time evolution of spectral wave energy density, $|E_x(t,k_x)|^2$, versus time, $\omega_{pe}t$, in the same format as Fig. 2. Panel (b) displays the time history of first six harmonics mode intensities in the same format as Fig. 3, and in panel (c) the plot of wave spectrum, $|E_x(k_x)|^2$, is shown versus k_x, which corresponds to $\omega_{pe}t=819.2$. The initial wave spectrum is also shown for the sake of comparison. Note that although at $t=0$, there should only be a single mode at $k_x=k_1$, the small but finite ($\propto 10^{-35}$) noise level is owing to

the roundoff error inherent with any digital computation. We also plotted an $x-v_x$ phase–space diagram at $\omega_{pe}t=409.6$ in panel (d).

Note from Fig. 8(b), that because there are practically no wave power at wave numbers other than $k_x=k_1$, the sea of initial perturbation which obscures the very early-time behavior associated with the harmonic modes is absent in the present case. As a result, one can clearly identify each harmonic mode as they begin to grow from small noise level. As straight lines which represent the linear theory demonstrate, the very early-time behavior of harmonic growths is in excellent agreement with the theory. However, since the coherent initial input is in flagrant violation of the assumption of quasilinear theory which is applicable only for a broadband spectrum, the subsequent dynamics is very different from the simple quasilinear theory prediction. Indeed, as panel (b) shows, the intensities associated with the harmonics show amplitude modulations, which must be due to coherent nonlinear physical effects. Such a modulation was also present to some degree in the case of power-law initial fluctuations, as Fig. 3 shows. However, the present Fig. 8(b) demonstrates much more prominent amplitude modulations.

The final spectrum shown in Fig. 8(c) is of course very different when compared with Fig. 7, since Fig. 8(c) is comprised of discrete multiple peaks. This shows that the system retains the memory of the initial condition. However, the striking fact is that if we connect the peaks of the individual spikes (minus the enhanced fundamental peak), we again obtain a rough estimate of power-law-like dependence with index -5 or -6 in the range $10^0<k_xV_d/\omega_{pe}<10^1$.

It is noteworthy that this run corresponds to a coherent initial input, and yet, it leads to a qualitatively similar result in comparison with the case of broadband incoherent initial noise. Consequently, the present example may shed some light on the alternative mechanism of harmonic generation, i.e., the coherent nonlinear theory first proposed in the early 1970s. In our simulation, it is found that in the relatively early phase of the simulation run ($\omega_{pe}t=0\sim100$), when the harmonic growth is still largely dictated by linear theory, the spectrum of the electric field is characterized by a steep power-law with an approximate -15 index. However, in the final stage, the saturated spectrum features, -5 to -6 index. To understand the time evolution of spectral index, we focus on the nonlinear trapping dynamics. Note that although the primary $L1$ mode grows according to the linear theory, it is clear that in the present example, the saturation is achieved by nonlinear trapping, which occurs around $\omega_{pe}t=400$. The phase–space diagram in Fig. 8(d) clearly shows this, which leads to the diffusion of the electron beam over the velocity range specified by

$$\frac{\omega^{L1}(k_1)}{k_1}-V_T<v_x<\frac{\omega^{L1}(k_1)}{k_1}+V_T, \tag{12}$$

where $V_T=2\omega_T/k_1$ and ω_T is given by

$$\omega_T=\sqrt{\frac{k_1|q_e||E_x(k_1)|}{m_e}}. \tag{13}$$

Coincident with the trapping, around $\omega_{pe}t\sim200$ and beyond, it is seen that the harmonic mode amplitudes rapidly increase with the effective amplification rates well above those predicted by quasilinear theory (this behavior is also seen in the case of incoherent run, Fig. 3, to some extent). A possible mechanism for such a rapid growth of the harmonics beyond $\omega_{pe}t\sim200$ is the effects due to the nonlinear trapping process, which creates a phase–space vortex rich in harmonic content. As a consequence, the modes with wave numbers, k_2, k_3, k_4, k_5, and k_6, experience additional enhanced amplification, thus yielding the eventual power-law index of $-5--6$.

V. DISCUSSIONS AND CONCLUSIONS

The results we have discussed thus far indicate the importance of the harmonic generation as a new way of approaching the Langmuir turbulence. The quasi-power-law spectrum associated with the saturated wave energy shows that it is natural for the Langmuir turbulence involving the harmonics to form a power-law distribution in wave energy spectrum. According to the theory originally developed by Yoon,[43] and generalized in paper II, the evolution equation for the spectral wave energy density for harmonic Langmuir mode, $I_n\equiv I_{Ln}(\mathbf{k})=|E_{Ln}(\mathbf{k})|^2$, is governed by an equation of the form [see also Eq. (11)],

$$\partial I_n/\partial t=\Gamma_n I_n. \tag{14}$$

As Fig. 3 and Eq. (9) show, the theoretical amplification rate agrees well with the simulation, at least during the early phase of the evolution. Thus, the above equation appears to describe the time evolution of the harmonic modes quite satisfactorily in an overall sense.

However, the above equation requires a finite level of harmonics at the outset, but such a level becomes a free parameter in our theory. Moreover, the final outcome of the solution highly depends on the initial condition, since the equation is essentially linear. For this reason, we had to manipulate the initial condition very carefully to produce the desired final solution in paper II, in order to reproduce the saturation wave spectrum which is consistent with the laboratory experiment[32,33] as well as with the Vlasov simulation shown in the present paper.

In the simulation, on the other hand, regardless of the form of the initial wave level, the system seems to readjust itself in two crucial ways. First, it damps out the ''unwanted'' noises early on in the simulation such that, even if we start the run with a ''wrong'' form of initial wave spectrum, the system self-regulates to create the true modes. This is evident from the initial rapid damping of the modes seen in Fig. 3, for instance. Then, once the true modes are generated at relatively early time, the subsquent internal dynamics seems to limit an unchecked growth of the modes (particularly for the higher harmonics with high linear growth rates), most likely through some mode couplings (as evidenced by the amplitude modulations seen in Figs. 3 and 8), which the incoherent turbulence theory may not be able to explain, if they involve coherent nonlinear dynamics. In the end, the beam–

plasma system produces a quasi-power-law spectrum with an apparently universal spectral index of -5 to -6.

Therefore, the crucial outstanding issues from the standpoint of theory, are to determine the initial level of the harmonic fluctuations in a self-consistent manner, or equivalently, incoporate the source term, S_n, on the right-hand side of Eq. (14),

$$\partial I_n/\partial t = \Gamma_n I_n + S_n,$$

and to include the mode-coupling terms on the right-hand side, so as to limit the unchecked growth of the high-harmonic modes,

$$\partial I_n/\partial t = \Gamma_n I_n + S_n + \sum_m a_{n,m} I_n I_m.$$

These are not trivial issues, however. The physical origin of the source can be attributed to either the generalized spontaneous fluctuations, or higher-order nonlinear correction terms which may lead to the forced nonlinear perturbation rich in harmonic content. The mode-coupling terms may involve particle trapping and coherent nonlinear dynamics, which the generalized weak turbulence theory cannot handle (yet). As such, while the theory and simulation show remarkable agreements on many aspects, such as the simulated wave dispersion relation and theoretical curves (which proves that treating the harmonic modes as turbulent eigenmodes is justified), the initial growth property, etc., there also remain a number of unresolved issues, as just outlined briefly. These are, of course, the subject of future research. However, we cannot overemphasize the fact that although the incoherent turbulence theory excludes the trapping effects at the outset, it is remarkable that the prediction of the nonlinear dispersion relation for the harmonics and the early-time growth behavior are in remarkable agreement with the simulation, even for a coherent initial input (Fig. 8).

ACKNOWLEDGMENTS

The work by T.U. was supported by grant-in-aid 03821 for research fellows of the Japan Society for the Promotion of Science (JSPS). The research carried out at the University of Maryland was supported by Department of Energy (DOE) grant DE-FG02-00ER54584. R.G. acknowledges support from the Brazilian agencies Conselho Nacional de Desenvolvimento Científico e Tecnológico (CNPq) and Fundação de Amparo à Pesquisa do Estado do Rio Grande do Sul (FAPERGS).

[1] A. A. Vedenov, E. P. Velikhov, and R. Z. Sagdeev, Nucl. Fusion **1**, 82 (1961).
[2] A. A. Vedenov, E. P. Velikhov, and R. Z. Sagdeev, Nucl. Fusion Suppl. **2**, 465 (1962).
[3] W. E. Drummond and D. Pines, Nucl. Fusion Suppl. **3**, 1049 (1962).
[4] B. B. Kadomtsev, *Plasma Turbulence* (Academic, New York, 1965).
[5] R. Z. Sagdeev and A. A. Galeev, *Nonlinear Plasma Theory* (Benjamin, New York, 1969).
[6] V. N. Tsytovich, *Nonlinear Effects in a Plasma* (Plenum, New York, 1970).
[7] R. C. Davidson, *Methods in Nonlinear Plasma Theory* (Academic, New York, 1972).
[8] A. I. Akhiezer, I. A. Akhiezer, R. V. Polovin, A. G. Sitenko, and K. N. Stepanov, *Plasma Electrodynamics. Vol. 2. Nonlinear Theory and Fluctuations* (Pergamon, New York, 1975).
[9] V. N. Tsytovich, *An Introduction to the Theory of Plasma Turbulence* (Pergamon, New York, 1977).
[10] A. G. Sitenko, *Fluctuations and Nonlinear Wave Interactions in Plasmas* (Pergamon, New York, 1982).
[11] J. M. Dawson and R. Shanny, Phys. Fluids **11**, 1506 (1968).
[12] R. L. Morse and C. W. Nielson, Phys. Fluids **12**, 2418 (1969).
[13] G. Joyce, G. Knorr, and T. Burns, Phys. Fluids **14**, 797 (1971).
[14] J. Denavit and W. L. Kruer, Phys. Fluids **14**, 1782 (1971).
[15] T. P. Armstrong and D. Montgomery, Phys. Fluids **12**, 2094 (1969).
[16] W. E. Drummond, J. H. Malmberg, T. M. O'Neil, and J. R. Thompson, Phys. Fluids **13**, 2422 (1970).
[17] T. M. O'Neil, J. H. Winfrey, and J. H. Malmberg, Phys. Fluids **14**, 1204 (1971).
[18] T. M. O'Neil and J. H. Winfrey, Phys. Fluids **15**, 1514 (1972).
[19] A. Simon and M. H. Rosenbluth, Phys. Fluids **19**, 1567 (1976).
[20] A. Simon, Phys. Fluids **20**, 79 (1977).
[21] A. L. Throop and R. R. Parker, Phys. Fluids **22**, 491 (1979).
[22] T. H. Dupree, Phys. Fluids **9**, 1733 (1966).
[23] A. A. Galeev, Phys. Fluids **10**, 1041 (1967).
[24] S. A. Orszag and R. H. Kraichnan, Phys. Fluids **10**, 1720 (1967).
[25] J. Weinstock, Phys. Fluids **12**, 1045 (1969).
[26] B. B. Kadomtsev and O. P. Pogutse, Phys. Fluids **14**, 2470 (1971).
[27] T. H. Dupree, Phys. Fluids **15**, 334 (1972).
[28] T. Boutros-Ghali and T. H. Dupree, Phys. Fluids **24**, 1839 (1981).
[29] K. Theilhaber, G. Laval, and D. Pesme, Phys. Fluids **30**, 3129 (1987).
[30] C. T. Dum, J. Geophys. Res. **95**, 8095 (1990); **95**, 8111 (1990); **95**, 8123 (1990).
[31] Y. Omura, H. Matsumoto, T. Miyake, and H. Kojima, J. Geophys. Res. **101**, 2685 (1996).
[32] J. R. Apel, Phys. Rev. Lett. **19**, 744 (1967).
[33] J. R. Apel, Phys. Fluids **12**, 640 (1969).
[34] J. H. Malmberg and C. B. Wharton, Phys. Fluids **12**, 2600 (1969).
[35] K. Mizuno and S. Tanaka, Phys. Rev. Lett. **29**, 45 (1972).
[36] K. W. Gentle and J. Lohr, Phys. Fluids **16**, 1464 (1973).
[37] H. Mori, J. Phys. Soc. Jpn. **35**, 592 (1973).
[38] M. Seidl, W. Carr, D. Boyd, and R. Jones, Phys. Fluids **19**, 78 (1976).
[39] R. W. Boswell and P. J. Kellogg, Geophys. Res. Lett. **10**, 565 (1983).
[40] X. Llobet, W. Bernstein, and A. Konradi, J. Geophys. Res. **90**, 5187 (1985).
[41] P. J. Kellogg, S. J. Monson, W. Bernstein, and B. A. Whalen, J. Geophys. Res. **91**, 12065 (1986).
[42] W. M. Manheimer, Phys. Fluids **14**, 579 (1971).
[43] P. H. Yoon, Phys. Plasmas **7**, 4858 (2000).
[44] R. Gaelzer, L. F. Ziebell, and P. H. Yoon, Phys. Plasmas **9**, 96 (2002).
[45] B. Goldstein, W. Carr, B. Rosen, and M. Seidl, Phys. Fluids **21**, 1569 (1978).
[46] P. L. Pritchett and J. M. Dawson, Phys. Fluids **26**, 1114 (1983).
[47] A. J. Klimas, J. Geophys. Res. **88**, 9081 (1983).
[48] K. Akimoto, H. L. Rowland, and K. Papadopoulos, Phys. Fluids **31**, 2185 (1988).
[49] A. J. Klimas, J. Geophys. Res. **95**, 14905 (1990).
[50] K.-I. Nishikawa and I. H. Cairns, J. Geophys. Res. **96**, 19343 (1991).
[51] L. Yin, M. Ashour-Abdalla, M. El-Alaoui, J. M. Bosqued, and J. L. Bougeret, J. Geophys. Res. **103**, 29619 (1998).
[52] D. Schriver, M. Ashour-Abdalla, V. Sotnikov, P. Hellinger, V. Fiala, R. Bingham, and A. Mangeney, J. Geophys. Res. **105**, 12919 (2000).
[53] Y. Kasaba, H. Matsumoto, and Y. Omura, J. Geophys. Res. **106**, 18693 (2001).
[54] C. G. Cheng and G. Knorr, J. Comput. Phys. **22**, 330 (1976).
[55] M. M. Shoucri and R. R. J. Gagne, J. Comput. Phys. **27**, 315 (1978).
[56] T. Yabe, T. Ishikawa, P. Y. Wang, T. Aoki, Y. Kadota, and R. Ikeda, Comput. Phys. Commun. **66**, 233 (1991).
[57] T. Nakamura and T. Yabe, Comput. Phys. Commun. **120**, 122 (1999).
[58] V. E. Zakharov, Sov. Phys. JETP **35**, 908 (1972).
[59] P. A. Robinson and D. L. Newman, Phys. Fluids B **2**, 2999 (1990).
[60] A. F. Viñas, H. K. Wong, and A. J. Klimas, Astrophys. J. **528**, 509 (2000).